Inorganic Chemistry

Article

pubs.acs.org/IC

Iridium(III) Complexes with Phenyl-tetrazoles as Cyclometalating Ligands

Filippo Monti,[†] Andrea Baschieri,[‡] Isacco Gualandi,[‡] Juan J. Serrano-Pérez,[§] José M. Junquera-Hernández,[§] Domenica Tonelli,[‡] Andrea Mazzanti,[‡] Sara Muzzioli,[‡] Stefano Stagni,[‡] Cristina Roldan-Carmona,[§] Antonio Pertegás,[§] Henk J. Bolink,[§] Enrique Ortí,*[,§] Letizia Sambri,*[,‡] and Nicola Armaroli*[,†]

[†]Istituto per la Sintesi Organica e la Fotoreattività, Consiglio Nazionale delle Ricerche, Via P. Gobetti, 101, I-40129, Bologna, Italy
[‡]Dipartimento di Chimica Industriale "Toso Montanari", Università di Bologna, Viale Risorgimento 4, I-40136, Bologna, Italy
[§]Instituto de Ciencia Molecular, Universidad de Valencia, Catedrático José Beltrán 2, E-46980, Paterna, Spain

Supporting Information

ABSTRACT: Ir(III) cationic complexes with cyclometalating tetrazolate ligands were prepared for the first time, following a two-step strategy based on (i) a silver-assisted cyclometalation reaction of a tetrazole derivative with $IrCl_3$ affording a bis-cyclometalated solvato-complex **P** ($[Ir(ptrz)_2(CH_3CN)_2]^+$, Hptrz = 2-methyl-5-phenyl-2*H*-tetrazole); (ii) a substitution reaction with five neutral ancillary ligands to get $[Ir(ptrz)_2L]^+$, with L = 2,2′-bypiridine (**1**), 4,4′-di-*tert*-butyl-2,2′-bipyridine (**2**), 1,10-phenanthroline (**3**), and 2-(1-phenyl-1*H*-1,2,3-triazol-4-yl)pyridine (**4**), and $[Ir(ptrz)_2L_2]^+$, with L = *tert*-butyl isocyanide (**5**). X-ray crystal structures of **P**, **2**, and **3** were solved. Electrochemical and photophysical studies, along with density functional theory calculations, allowed a comprehensive rationalization of the electronic properties of **1**−**5**. In acetonitrile at 298 K, complexes equipped with bipyridine or phenanthroline ancillary ligands (**1**−**3**) exhibit intense and structureless emission bands centered at around 540 nm, with metal-to-ligand and ligand-to-ligand charge transfer (MLCT/LLCT) character; their photoluminescence quantum yields (PLQYs) are in the range of 55−70%. By contrast, the luminescence band of **5** is weak, structured, and blue-shifted and is attributed to a ligand-centered (LC) triplet state of the tetrazolate cyclometalated ligand. The PLQY of **4** is extremely low (<0.1%) since its lowest level is a nonemissive triplet metal-centered (^{3}MC) state. In rigid matrix at 77 K, all of the complexes exhibit intense luminescence. Ligands **1**−**3** are also strong emitters in solid matrices at room temperature (1% poly(methyl methacrylate) matrix and neat films), with PLQYs in the range of 27−70%. Good quality films of **2** could be obtained to make light-emitting electrochemical cells that emit bright green light and exhibit a maximum luminance of 310 cd m^{-2}. Tetrazolate cyclometalated ligands push the emission of Ir(III) complexes to the blue, when compared to pyrazolate or triazolate analogues. More generally, among the cationic Ir(III) complexes without fluorine substituents on the cyclometalated ligands, **1**−**3** exhibit the highest-energy MLCT/LLCT emission bands ever reported.

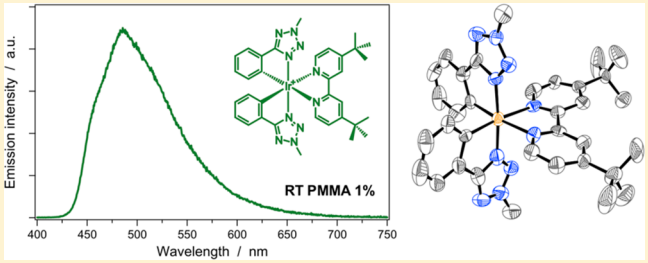

INTRODUCTION

Ir(III) cyclometalated (C^N) complexes continue to be the most widely utilized class of triplet emitters in flat electroluminescent devices such as organic light-emitting diodes (OLEDs) and light-emitting electrochemical cells (LECs).[1−11] Their high luminescence quantum yield and unsurpassed versatility in tuning the emission color throughout the entire visible spectral window by ligand design have prompted an impressive amount of work on this class of metal complexes worldwide. Over the past 20 years, a huge amount of blue, green, and red Ir(III) emitters, made of both homoleptic $[Ir(C^N)_3]$- and heteroleptic $[Ir(C^N)_2(L^L)]^{0/+}$-type complexes, has been produced.[1,8,12] The former are electrically neutral and are targeted to OLED technology,[7,13] whereas the latter are normally monocationic (L^L typically denotes a neutral chelating ligand) and hence suitable for LEC devices.[5] Emission color tuning is conceptually simple and is accomplished by modifying the energy gap separating the highest-occupied (HOMO) and lowest-unoccupied molecular orbital (LUMO): blue shifting (i.e., bandgap widening) is obtained through stabilization of the HOMO and/or destabilization of the LUMO, and red shifting (bandgap narrowing) is accomplished with the opposite approach.[1,5]

In the case of Ir(III) complexes, the HOMO orbital is predominantly located on the cyclometalating ligand, whereas the LUMO is usually centered on the ancillary diimino N^N ligand, as long as it possesses low-lying π^* orbitals such as 2,2′-bipyridine (bpy) or 1,10-phenanthroline (phen), as is very often the case.[1] From the preparative standpoint, it is much

Received: May 2, 2014
Published: July 8, 2014

   dx.doi.org/10.1021/ic500999k | *Inorg. Chem.* 2014, 53, 7709−7721

easier to chemically modify the ancillary ligand, which is prepared independently and eventually attached to the cyclometalated Ir(III) μ-dichloro-bridged dimer $[(C\hat{}N)_2Ir(\mu\text{-}Cl)]_2$ that contains the four selected cyclometalated units. Therefore, in the vast majority of cases, color tuning has been pursued through modification of the ancillary ligand.[14−17]

The less-frequently investigated modification of the C^N ligand has been primarily addressed to the preparation of blue-emitting complexes, which are presently the key target as active materials for electroluminescent devices.[15,18−26] This is because wide HOMO−LUMO gaps are more difficult to obtain and, moreover, the high energy levels of blue emitters tend to be reactive under the device operating conditions.[1]

Two main modification strategies of the C^N ligand have been pursued to stabilize the HOMO and shift the emission band of Ir(III) complexes to the blue: (i) addition of electron-withdrawing groups, typically fluorines,[27] and (ii) reduction of the ring size of the aromatic N-heterocycle. As far as the latter approach is concerned, several examples of Ir(III) complexes with cyclometalating ligands entailing 5-membered nitrogen-containing rings have been reported, namely, 1-aryl-1,2-pyrazoles,[18,28−30] and phenyl imidazoles.[31] In addition, a few aryl triazoles have been also proposed, such as 5-aryl-1,2,4-triazoles[32] and aryl-1,2,3-triazoles.[33−38] However, only cationic Ir(III) complexes with 1-phenyl-1,2-pyrazoles led to a blue shift of the emission compared to analogues with the prototypical 2-phenylpyridine ligand — for instance: $[Ir(ppy)_2(bpy)]^+$ (Hppy = 2-phenylpyridine), λ_{max} = 602 nm;[21] $[Ir(ppz)_2(bpy)]^+$ (Hppz = 1-phenyl-1,2-pyrazole), λ_{max} = 563 nm.[28] Surprisingly, the use of phenyl-triazoles did not further blue shift the emission band ($[Ir(phtl)_2(bpy)]^+$ (Hphtl = 1-phenyl-1,2,3-triazole), λ_{max} = 580 nm).[34] Therefore, an increase of the number of nitrogen atoms on the 5-membered heterocycle does not warrant an increase of the emission energy of the complexes, although one might expect that electron-rich triazoles in C^N ligands should enhance the ligand field splitting of Ir(III) d orbitals.

This unexpected result prompted us to explore the possibility of using the 5-phenyltetrazole cyclometalating ligand that, according to a preliminary appraisal by quantum chemical calculations, should have afforded complexes with blue-shifted emissions compared to the pyrazole-based analogue $[Ir(ppz)_2(bpy)]^+$. However, to the best of our knowledge, 5-aryltetrazoles had never been used as cyclometalating ligands for Ir(III) complexes, probably because the cyclometalation of the iridium metal center by the 5-aryltetrazole ligand cannot be directly accomplished (*vide infra*).

Herein, we present not only the first series of iridium(III) phenyltetrazolate complexes, but also the first example of a silver-assisted cyclometalation reaction of a tetrazole derivative starting directly from $IrCl_3$. In this way we obtained the bis-cyclometalated phenyl-tetrazole Ir(III) solvato complex $[Ir(ptrz)_2(CH_3CN)_2]^+$ (**P**, Hptrz = 2-methyl-5-phenyl-2*H*-tetrazole), which was used as a precursor for the preparation of five new Ir-iTMCs (**1**−**5**; iTMCs = ionic transition-metal complexes) by reaction with different neutral ancillary ligands. The complete series of complexes based on the novel Hptrz cyclometalating ligand is reported in Chart 1, along with the precursor **P**.

As correctly anticipated by our preliminary theoretical assessment, this series of compounds displays markedly blue-shifted emission bands ($\lambda_{max} \approx$ 530 nm), if compared to other nonfluorinated Ir(III) complexes (**A1**, **B1**, and **C1**, Chart 2).[21,28,34] In addition to that, some of them (**1**−**3**) show

Chart 1. Tetrazole-Based Ionic Ir(III) Complexes Investigated in This Work

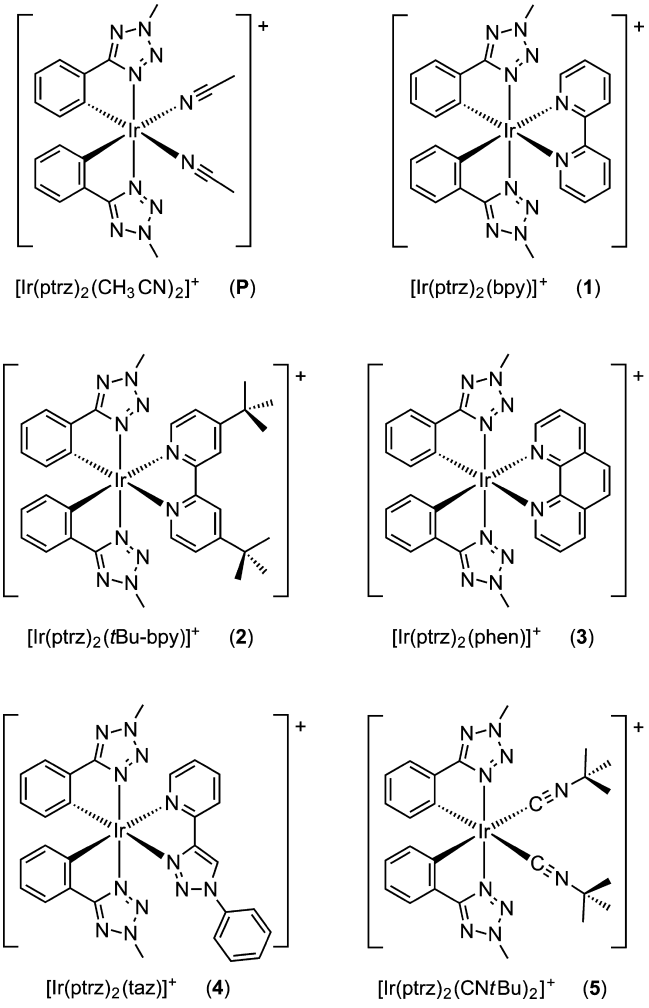

remarkably high emission quantum yields (~70%) that are comparable only to some polyfluorinated Ir-iTMCs (e.g., **A2**).[34]

There are at least three main advantages in using the cyclometalating ligands herein presented for the synthesis of cationic Ir(III) complexes: (i) the high-field nature of phenyl-tetrazole that can lead to blue-shifted emissions without the need to use electron-deficient polyfluorinated ligands while, at the same time, preserving the relatively short-lived and highly emissive metal-to-ligand charge transfer (MLCT) nature of the emitting states; (ii) the absence of reactive $C(sp^2)$−F bonds that normally afford instability when the complex is used in LECs;[20,39,40] (iii) the higher radiative rate constants compared to standard blue-emitting fluorine-free Ir-iTMCs (with, e.g., isocyanide ancillary ligands),[22,23,26] which allows optimized performance in devices preventing exciton quenching.[22,26]

EXPERIMENTAL SECTION

Synthesis of 2-Methyl-5-phenyl-2*H*-tetrazole (Ia, Scheme 1). A solution of 5-phenyl-2*H*-tetrazole (**I**) (1.0 g, 6.8 mmol) in CH_3CN (70 mL) was treated with K_2CO_3 (3.8 g, 27.4 mmol) followed by addition of methyl iodide (0.86 mL, 13.6 mmol), according to a described procedure.[42] The reaction was stirred at reflux for 72 h, then it was cooled to room temperature, the residual solid was filtered off, and the solution was concentrated in vacuo to give a dark oil. The oil was then purified by column chromatography on silica eluting with

dx.doi.org/10.1021/ic500999k | Inorg. Chem. 2014, 53, 7709−7721

Chart 2. Selected Archetypal Examples of Ir-iTMCs Having 2,2′-Bipyridine as Neutral Ancillary Ligand[21,28,34,41]

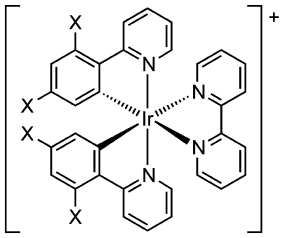

X = H [Ir(ppy)$_2$(bpy)]$^+$ (**A1**)
X = F [Ir(dfppy)$_2$(bpy)]$^+$ (**A2**)

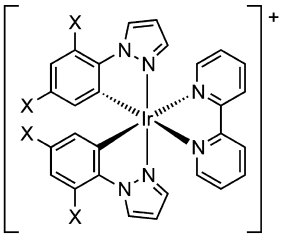

X = H [Ir(ppz)$_2$(bpy)]$^+$ (**B1**)
X = F [Ir(dfppz)$_2$(bpy)]$^+$ (**B2**)

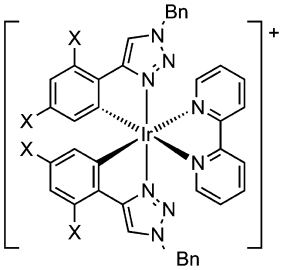

X = H [Ir(phtl)$_2$(bpy)]$^+$ (**C1**)
X = F [Ir(dfphtl)$_2$(bpy)]$^+$ (**C2**)

Emission maximum at 298 K

	in CH_2Cl_2	*in CH_3CN*
A1	595 nm[c]	602 nm[a]
A2	535 nm[c]	527 nm[a]
B1	554 nm[b]	563 nm[b]
B2*	484 nm[b]	495 nm[b]
C1	- - - -	580 nm[a]
C2	- - - -	514 nm[a]

[a] *from ref.* 31.
[b] *from ref.* 25.
[c] *from ref.* 38.
* *Data for complexes with tBu-bpy.*

Scheme 1. Reactivity of 5-Phenyltetrazoles 1a−c under Various Conditions

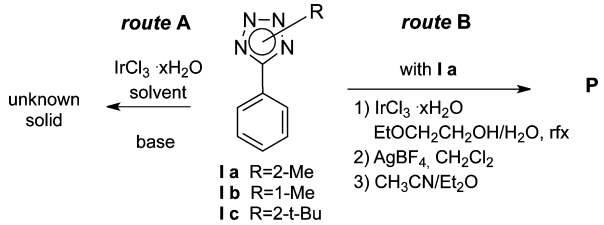

CH_2Cl_2/petroleum ether (4/6) and then CH_2Cl_2/EtOAc (98/2). Homogeneous fractions by thin-layer chromatography were combined and concentrated in vacuum to give 2-methyl-5-phenyl-2*H*-tetrazole (0.67 g, 59.1% yield, less polar spot) as a pale yellow solid [^{1}H NMR ($CDCl_3$) δ: 4.33 (s, 3H), 7.35−7.50 (m, 3H), 8.05−8.15 (m, 2H); ^{13}C NMR ($CDCl_3$) δ: 39.5 (CH_3), 126.8 (CH), 127.3 (C), 128.9 (CH), 130.3 (CH), 165.2 (C)] and 1-methyl-5-phenyl-2*H*-tetrazole (0.26 g, 23.7% yields) as a white solid [^{1}H NMR ($CDCl_3$) δ: 4.18 (s, 3H), 7.55−7.60 (m, 3H), 7.70−7.75 (m, 2H); ^{13}C NMR ($CDCl_3$) δ: 35.0 (CH_3), 123.8 (C), 128.6 (CH), 129.3 (CH), 131.3 (CH), 165.9 (C)].

Synthesis of Ir(III) Solvato Complex (P). The reactions were performed under N_2 and in the absence of light. The solvents were not dried but were deoxygenated by bubbling with N_2. The ligand 2-methyl-5-phenyl-2*H*-tetrazole (96 mg, 0.6 mmol) was dissolved in a 3:1 mixture of ethoxyethanol/water (4 mL), and then $IrCl_3{\cdot}xH_2O$ (60 mg) was added. The mixture was stirred overnight at 140 °C under N_2. After cooling, the obtained yellow solid was filtered, washed with water, dried, and dissolved in CH_2Cl_2 (15 mL). $AgBF_4$ (80 mg) was added, and the solution was vigorously stirred and then refluxed for 6 h. After cooling, the solution was filtered through a paper filter to remove AgCl and was evaporated to dryness. The resulting crude Ir(III) solvato complex was dissolved in CH_3CN, precipitated twice with Et_2O, and then crystallized from slow diffusion of Et_2O vapors in a CH_3CN solution to give colorless crystals of **P** (40 mg, 60% yield). ^{1}H NMR (crystals, CD_3OD) δ: 2.03 (s, 6H), 4.65 (s, 6H), 6.14 (d, 2H, J_{HH} = 7.5 Hz), 6.80 (dt, 2H, J_{HH} = 7.5 Hz, J_{HH} = 1.4 Hz), 6.92 (dt, 2H, J_{HH} = 7.5 Hz, J_{HH} = 1.2 Hz), 7.64 (d, 2H, J_{HH} = 7.5 Hz, J_{HH} = 1.4 Hz); ^{13}C NMR (precipitate, CD_3OD) δ: 40.8 (CH_3), 122.8 (CH), 123.6 (CH), 129.8 (CH), 130.0 (C), 133.1 (C), 133.6 (CH), 174.3 (C)]. Anal. Calcd for $C_{22}H_{23}BF_4IrN_{11}$ (721.18) (X-ray crystals): C, 36.61; H, 3.21; N, 21.36%. Found: C, 36.50; H, 3.08; N, 21.29%. Electrospray ionization mass spectrometry (ESI-MS$^+$): 593 (M − BF_4)$^+$; 552 (M − BF_4 − ACN) $^+$; 511 (M − BF_4 − 2ACN)$^+$.

Synthesis of Complexes 1−4. The solvato complex **P** (50 mg, 0.074 mmol) was dissolved in a 3:1 mixture of CH_2Cl_2/EtOH (4 mL), and then the appropriate bidentate diimino ligand (0.22 mmol) was added, that is, 2,2′-bypiridine (bpy), 4,4′-di-*tert*-butyl-2,2′-bipyridine (^{t}Bu-bpy), 1,10-phenanthroline (phen), and 2-(1-phenyl-1*H*-1,2,3-triazol-4-yl)pyridine (taz) for complexes **1**, **2**, **3**, and **4**, respectively. The mixture was stirred overnight at room temperature (RT), and then the solvent was evaporated. The solid was dissolved in acetone, precipitated with Et_2O, and the obtained solid was purified by column chromatography (CH_2Cl_2/MeOH = 98/2) to give pure complexes **1**−**4**.

*Complex **1** (42 mg, 75% yield).* ^{1}H NMR (CD_2Cl_2) δ: 4.27 (s, 6H), 6.24 (d, 2H, J_{HH} = 8.8 Hz), 6.98 (t, 2H, J_{HH} = 8.8 Hz), 7.05 (t, 2H, J_{HH} = 8.8 Hz), 7.36 (t, 2H, J_{HH} = 7.0 Hz), 7.70 (d, 2H, J_{HH} = 7.0 Hz), 8.00−8.10 (m, 4H), 8.51 (d, 2H, J_{HH} = 7.0); ^{13}C NMR (CD_2Cl_2) δ: 42.1 (CH_3), 123.6 (CH), 124.8 (CH), 125.1 (CH), 127.7 (CH), 129.2 (C), 131.5 (CH), 132.6 (CH), 140.2 (CH), 145.6 (C), 151.7 (CH), 156.7 (C), 174.6 (C). Anal. Calcd for $C_{26}H_{22}BF_4IrN_{10}$ (754.17): C, 41.37; H, 2.94; N, 18.57%. Found: C, 41.44; H, 2.85; N, 18.49%. ESI-MS$^+$: 667 (M − BF_4)$^+$.

*Complex **2** (44.3 mg, 70% yield).* ^{1}H NMR (CD_2Cl_2) δ: 1.45 (s, 18H), 4.37 (s, 6H), 6.33 (d, 2H, J_{HH} = 7.4 Hz), 7.06 (dt, 2H, J_{HH} = 7.4 Hz, J_{HH} = 1.7 Hz), 7.14 (dt, 2H, J_{HH} = 7.4 Hz, J_{HH} = 1.3 Hz), 7.43 (dd, 2H, J_{HH} = 5.8 Hz, J_{HH} = 1.9 Hz), 7.80 (dd, 2H, J_{HH} = 7.4 Hz, J_{HH} = 1.7 Hz), 8.02 (d, 2H, J_{HH} = 5.8 Hz), 8.30 (d, 2H, J_{HH} = 1.9 Hz); ^{13}C NMR (CD_2Cl_2) δ: 30.0 (CH_3), 35.6 (C), 41.6 (CH_3), 120.4 (CH), 123.5 (CH), 124.7 (CH), 124.8 (CH), 129.2 (C), 131.4 (CH), 132.5 (CH), 145.0 (C), 151.3 (CH), 156.3 (C), 164.2 (C), 174.7 (C). Anal. Calcd for $C_{35}H_{40}BF_4IrN_{10}Cl_2$ (950.25) (X-ray crystals): C, 44.20; H, 4.24; N, 14.74%. Found: C, 44.00; H, 4.15; N, 14.94%. ESI-MS$^+$: 779 (M − BF_4)$^+$.

*Complex **3** (31 mg, 54% yield).* ^{1}H NMR (CD_2Cl_2) δ: 4.17 (s, 6H), 6.35 (d, 2H, J_{HH} = 7.6 Hz), 7.02 (dt, 2H, J_{HH} = 7.5 Hz, J_{HH} = 1.6 Hz), 7.08 (dt, 2H, J_{HH} = 8.8 Hz, J_{HH} = 1.9 Hz), 7.36 (t, 2H, J_{HH} = 7.0 Hz), 7.70−7.75 (m, 4H), 8.02 (s, 2H), 8.33 (dd, 2H, J_{HH} = 5.5 Hz, J_{HH} = 1.9 Hz), 8.57 (dd, 2H, J_{HH} = 8.5 Hz, J_{HH} = 1.6 Hz); ^{13}C NMR (CD_2Cl_2) δ: 41.5 (CH_3), 123.7 (CH), 124.8 (CH), 126.0 (CH), 128.2 (CH), 129.4 (C), 131.1 (C), 131.4 (CH), 132.7 (CH), 138.7 (CH), 144.9 (C), 147.7 (C), 152.0 (CH), 174.6 (C). Anal. Calcd for $C_{29}H_{24}BF_4IrN_{10}Cl_2$ (862.12) (X-ray crystals): C, 40.36; H, 2.80; N, 16.24%. Found: C, 40.50; H, 2.89; N, 16.50%. ESI-MS$^+$: 691 (M − BF_4)$^+$.

*Complex **4** (25 mg, 42% yield).* ^{1}H NMR (CD_2Cl_2) δ: 4.29 (s, 3H), 4.30 (s, 3H), 6.27 (d, 2H, J_{HH} = 7.5 Hz), 6.90−7.10 (m, 4H), 7.22 (bt, 1H, J_{HH} = 6.7 Hz), 7.40−7.50 (m, 3H), 7.69 (dd, 2H, J_{HH} = 7.1 Hz, J_{HH} = 11.3 Hz), 7.78 (bd, 1H, J_{HH} = 7.1 Hz), 7.89 (d, 1H, J_{HH} = 5.2 Hz), 8.0 (bs, 1H), 8.5 (bs, 2H), 9.5 (s, 2H); ^{13}C NMR (CD_2Cl_2) δ: 41.6 (CH_3), 41.7 (CH_3), 120.8 (CH), 123.2 (CH), 123.5 (CH), 123.6 (CH), 124.1 (C), 124.3 (CH), 124.7 (CH), 125.6 (CH), 129.3 (C), 130.0 (CH), 130.2 (CH), 130.6 (CH), 131.3 (CH), 132.5 (CH), 133.0 (CH), 136.1 (CH), 140.0 (CH), 141.8 (C), 145.1 (C), 150.2 (C), 150.3 (C), 151.0 (CH), 159.3 (C), 174.4 (C), 174.8 (C). Anal. Calcd for $C_{29}H_{24}BF_4IrN_{12}$ (820.19): C, 42.43; H, 2.95; N, 20.49%. Found: C, 42.71; H, 2.87; N, 20.37%. ESI-MS$^+$:733 (M − BF_4)$^+$.

Synthesis of Complex 5. ***Caution!*** *tert-Butyl isocyanide is a foul-smelling volatile liquid; therefore, ensure adequate ventilation!* The solvato complex **P** (60 mg, 0.088 mmol) was dissolved in a 3:1 mixture of CH_2Cl_2/EtOH (4 mL), and *tert*-butyl isocyanide (CN^tBu, 0.88 mmol) was added. The mixture was left to stir overnight at 30 °C, and then the solvent was evaporated. The solid was dissolved in acetone, and the product was precipitated with Et_2O to give pure complex **5** (27 mg, 40% yield). ^{1}H NMR (CD_2Cl_2) δ: 1.44 (s, 18H), 4.70 (s, 6H), 6.15 (d, 2H, J_{HH} = 7.5 Hz), 7.01 (dt, 1H, J_{HH} = 7.5 Hz, J_{HH} = 1.6 Hz), 7.09 (dt, 2H, J_{HH} = 7.5 Hz, J_{HH} = 1.4 Hz), 7.76 (d, 2H, J_{HH} = 7.5 Hz); ^{13}C NMR (CD_2Cl_2) δ: 30.0 (CH_3), 42.2 (CH_3), 65.6 (C), 124.2

dx.doi.org/10.1021/ic500999k | *Inorg. Chem.* 2014, 53, 7709−7721

(CH), 124.8 (CH), 128.3 (C), 131.2 (CH), 131.3 (CH), 149.1 (C), 157.6 (C), 174.8 (C). Anal. Calcd for $C_{26}H_{32}BF_4IrN_{10}$ (764.25): C, 40.82; H, 4.22; N, 18.32%. Found: C, 41.02; H, 4.33; N, 18.27%. ESI-MS$^+$:677 $(M - BF_4)^+$.

Experimental details on the electrochemistry, photophysics, and LEC devices and computational details on density functional calculations are reported in the Supporting Information.

RESULTS AND DISCUSSION

Synthesis. Direct cyclometalation of phenylpyridines by Ir(III) derivatives is an established reaction that is widely exploited for the synthesis of hundreds of complexes.[43−45] The classical cyclometalating methods work well also with cyclometalating ligands containing 5-membered rings with two or three nitrogen atoms.[13,23−26,28−30]

Repeated attempts to obtain the classical dimer $(C^N)_2Ir(\mu\text{-}Cl)_2Ir(C^N)_2$ by direct reaction of $IrCl_3{\cdot}xH_2O$ with a N-substituted 5-phenyltetrazole as cyclometalating ligand following literature procedures[44,46] failed. On the other hand, the use of high-boiling solvents, such as glycerol or ethylene glycol, or the addition of a base did not bring any significant results. We always observed the formation of an unknown product, presumably a salt involving the ligand and $IrCl_3$,[47] without any cyclometalation (Scheme 1, route A).

Therefore, in an attempt to induce cyclometalation, an intermediate synthetic step consisting of the Ag(I)-mediated halide extraction was introduced.[47] Following this approach, the yellow solid obtained by refluxing **Ia** with $IrCl_3{\cdot}xH_2O$ in an ethoxyethanol/water mixture — whose ^{1}H NMR spectrum exactly matched that of the free ligand **1a** — was reacted with $AgBF_4$ in CH_2Cl_2 (Scheme 1, route B). The species obtained was treated with CH_3CN and Et_2O vapors, affording the cyclometalated solvato complex **P**, whose structure was resolved by X-ray diffraction.

A thorough choice of the nature and position of the tetrazole substituent was essential for the success of the reaction. Among the ligands tested, only 2-methyl-5-phenyltetrazole **Ia** gave satisfactory results. Indeed, when the methyl substituent is shifted to the 1-position (**Ib**, Scheme 1) the reaction does not occur. This is likely because 1-alkyl-5-phenyltetrazoles, either as "free"[48] or as coordinated ligands,[49] do not exhibit the preferentially coplanar arrangement of the aromatic rings that would be required for any ligand capable of coordinating a metal center through a bis-chelate geometry. Moreover, if the substituent is changed from methyl to *tert*-butyl, a C−H activation of an sp^3 C−H bond can compete with the cyclometalation of the arylic C−H bond, affording a complex mixture of products.

The reaction of the solvato complex **P** with the bidentate ligands bpy, ^{t}Bu-bpy, phen, and taz, under mild reaction conditions, gave complexes **1**−**4** (Scheme 2) in satisfactory yields. Similarly, complex **5** was obtained by treatment of **P** with an excess of CN^{t}Bu.

X-ray Characterization. Good-quality single crystals of **P**, **2**, and **3** were obtained by slow diffusion of Et_2O in CH_3CN and CH_2Cl_2 solutions. The X-ray structures of the solvato complex **P** and of complexes **2** and **3** showed the same arrangement of the two phenyl-tetrazole ligands around a pseudo-octahedral iridium ion. One of the phenyl-tetrazoles is bound to two equatorial positions of the octahedral Ir center, whereas the second one occupies an equatorial position with nitrogen and an axial position with carbon (Figure 1). This arrangement implies that the two nitrogens of the tetrazole

Scheme 2. Synthesis of Complexes 1−5 from P

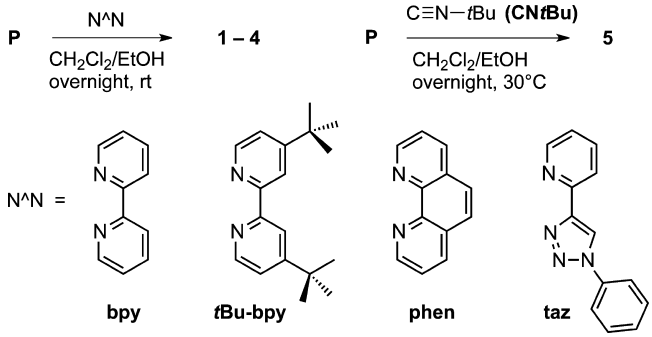

rings are mutually in a trans position. The two acetonitrile molecules of **P** fill the remaining equatorial and axial positions. During the final reaction step, the two acetonitrile molecules are displaced by the ancillary ligand (Figure 1).

The Ir−N and Ir−C distances are summarized in Table 1 and are very similar to other iridium complexes reported in the literature.[34,35,38,50−59] Therefore, the different geometry of the tetrazole with respect to heterocycles used previously does not alter the bonding distances.

Electrochemical Properties. The electrochemical behavior of **1**−**5** was investigated by cyclic voltammetry (CV) in acetonitrile (Figure 2). The nature of the ancillary ligands affects both the potentials and the reversibility of the redox processes. All compounds display at least one oxidation and two reduction processes. The formal half-wave potentials of the reversible processes and the peak potentials of the irreversible ones are reported in Table 2.

The CVs of **1**−**3** display one reversible wave in the cathodic side with a formal potential of approximately −1.8 V, along with another irreversible reduction process at around −2.6 V. The former is a monoelectronic process, as evidenced from a ΔE_p value of ∼70 mV. As far as the anodic side is concerned, **1**−**3** exhibit only one oxidation process around +1.2 V, which appears irreversible at a scan rate of 0.05 V s^{-1}. As the scan rate is increased, the backward peak indicates a complex kinetics of this process (see Figure S1 in the Supporting Information for complex **1**). From the graphs of normalized peak currents versus the square root of the scan rate, an $E_{rev}CE$-type kinetics is determined, that is, a reversible electrochemical process followed by a chemical reaction that in turn is followed by another electrochemical process. At a scan rate of 10 V s^{-1} the shapes of the voltammograms are typical of a quasi-reversible process; therefore, the calculated formal potentials can be considered as thermodynamic data. Moreover, the appearance of a backward wave for the process on the anodic side for **2** appears at a lower scan rate (0.1 V s^{-1}) than that needed for **1** and **3** (0.5 V s^{-1}). This observation suggests that, under the conditions of the electrochemical experiments, the species formed upon oxidation of **2** is more stable than those formed with **1** and **3**. (0.5 V s^{-1}).

The CV of **4** displays two cathodic waves at −2.226 and −2.68 V and one anodic wave at +1.256 V. At 0.05 V s^{-1} only the forward peaks are present for all the processes, but by increasing the scan rate, the backward peaks of the less cathodic process and of the anodic one appear. The mechanisms of the electrochemical processes are $E_{rev}C$ and $E_{rev}CE$, respectively (see footnotes in Table 2).

The CV of **5** exhibits two cathodic waves at −2.504 and −2.71 V and an anodic feature at +1.569 V that do not display

dx.doi.org/10.1021/ic500999k | Inorg. Chem. 2014, 53, 7709−7721

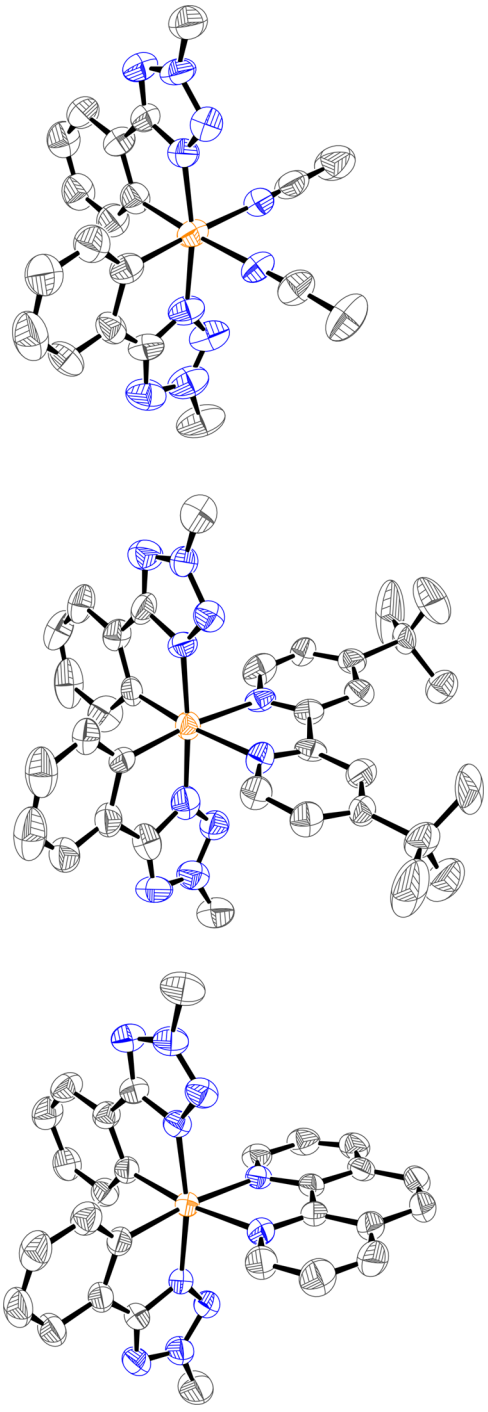

Figure 1. Experimental X-ray structures of the solvato complex **P** and of complexes **2** and **3**. ORTEP representations are at the 50% probability. Counter anion, solvents, and hydrogen atoms are omitted for the sake of clarity.

the corresponding backward wave either at 0.05 V s^{-1} or at higher scan rates, suggesting irreversibility. In such a case, the peak potentials, which can be considered only a rough estimation of the thermodynamic values, are reported in Table 2.

Overall, the electrochemical data suggest that the nature of the ancillary ligand affects the first reduction potentials more remarkably than the oxidation potentials. Indeed, the first reduction of the Ir complexes usually occurs on the ancillary ligands, while the oxidation is centered on the Ir-aryl moiety.

Table 1. Selected Data from X-ray Analysis

	bite angle (deg) C^N	bite angle (deg) N^N	Ir–N^a (Å)	Ir–C (Å)	Ir–N^b (Å)
P	80.11	87.90	2.024	2.034	2.117
	80.01		2.041	2.046	2.108
3	79.49	77.52	2.025	2.034	2.139
	79.62		2.017	2.030	2.131
2[c]	80.30	75.57	2.044	1.998	2.135
	80.83		2.011	2.016	2.145
	77.06	77.37	1.997	2.074	2.120
	77.91		2.000	2.084	2.112

[a]Tetrazole nitrogen. [b]Nitrogens of the ancillary ligand. [c]Two independent molecules are present in the unit cell.

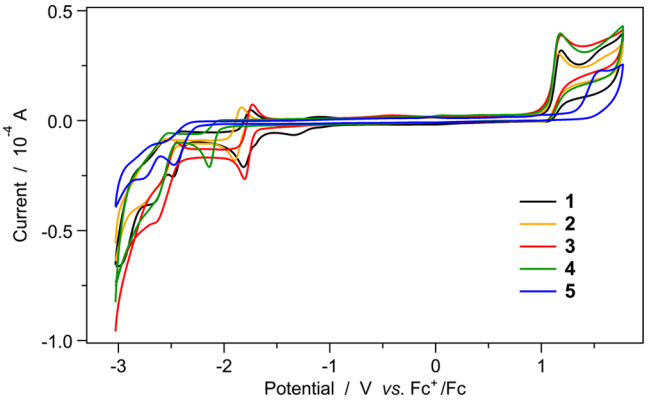

Figure 2. Cyclic voltammograms of **1**–**5** recorded at a scan rate of 0.05 V s^{-1} in acetonitrile.

Table 2. Electrochemical Properties of 1–5

	$E_{red1}^{\circ\prime}$ (V)[a]	$E_{red2/3}^{\circ\prime}$ (V)[a]	$E_{ox}^{\circ\prime}$ (V)[a]
1	−1.785 (rev.)	−2.49[b]/−2.71[b]	+1.156 (E_{rev}CE)
2	−1.866 (rev.)	−2.64[b]	+1.139 (E_{rev}CE)
3	−1.769 (rev.)	−2.69[b]	+1.179 (E_{rev}CE)
4	−2.226 (E_{rev}C)	−2.68[b]	+1.256 (E_{rev}CE)
5	−2.504[b] (irrev.)	−2.71[b]	+1.569[b] (irrev.)

[a]Potential values vs Fc^+/Fc. [b]Peak potential value. rev. = reversible; irrev. = irreversible; E_{rev}C = reversible process followed by chemical reaction; E_{rev}CE = reversible process followed by chemical reaction and a second electron transfer process. $E_{ox}^{\circ\prime}$ refers to the oxidation process; $E_{red1}^{\circ\prime}$ and $E_{red2/3}$ refer to the first and second/third reduction waves, respectively. The first electrochemical cathodic and anodic processes were monoelectronic for all the investigated compounds.

The redox gap of the whole series (calculated as the difference between the formal potentials of the cathodic and anodic systems) spans over a wide range, namely, ∼2.9–4.1 V. As far as the electrochemical behavior of **1**–**3** is concerned, we can make the following observations: (i) the first reduction process occurs at less cathodic potentials than that of **4** because the triazole moiety is more electron-rich than bipyridine and phenanthroline;[60] (ii) the electrochemistry of **5** is highly affected by the *tert*-butyl isocyanide ligands that have a strong electron-withdrawing character, which lowers the energy of the Ir-aryl centered HOMO.[26] Notably, **5** exhibits by far the highest redox gap of the series.

The excited-state electrochemical potentials[61] were also estimated for **1**, taken as a model for **1**–**3** that are characterized by similar spectroscopic and electrochemical features. These quantities are easily calculated from the ground-state electro-

dx.doi.org/10.1021/ic500999k | Inorg. Chem. 2014, 53, 7709–7721

chemical potentials and the spectroscopic energy ($E^{\circ\circ}$, in eV units) related to the involved transition.[62] The resulting formal potentials for the MLCT excited-state couples of **1** (vs Fc/Fc^+) are +0.965 ($[Ir(ptrz)_2(bpy)]^{+*} + e^- \rightleftharpoons [Ir(ptrz)_2(bpy)]$) and −1.594 V ($[Ir(ptrz)_2(bpy)]^{2+} + e^- \rightleftharpoons [Ir(ptrz)_2(bpy)]^{+*}$), respectively. Thus, the excited state of complex **1** ($[Ir(ptrz)_2(bpy)]^{+*}$) is a moderately strong oxidant as well as a very strong reductant. The latter finding is in line with many other Ir(III) complexes having similar triplet energy, whereas the excited state oxidative power of **1** is particularly high when systematically compared to Ir(III) complexes previously reported.[16]

Theoretical Calculations: Electronic Ground State. The molecular and electronic structures of complexes **1**−**5** were investigated by density functional theory (DFT) calculations at the B3LYP/(6-31G**+LANL2DZ) level considering solvent effects (see the Supporting Information for full computational details). The geometries of the complexes in the electronic ground state (S_0) were fully optimized, and the values obtained for the bond lengths and bond angles defining the coordination sphere of the iridium center are collected in Table S2 in the Supporting Information. Both the ancillary N^N ligand and the cyclometaling $ptrz^-$ ligands remain mainly planar and define a near-octahedral coordination for the Ir metal. The maximum deviation from planarity (1.32°) is found for the ^{t}Bu-bpy ligand in complex **2**. The bite angles formed by the $ptrz^-$ ligands with the Ir center are always around 79.3°, in good agreement with the X-ray values collected in Table 1, and are similar to those previously reported for iridium(III) complexes bearing 1-phenylpyrazole (Hppz) ligands.[63]

Figure 3 displays the energy and the atomic orbital composition calculated for the HOMO and LUMO of

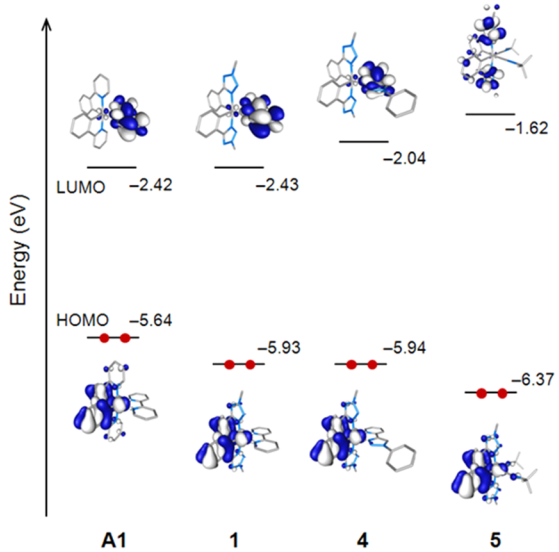

Figure 3. Energy diagram showing the isovalue contours (±0.03 au) and the energy values calculated for the HOMO and LUMO of complexes **A1**, **1**, **4**, and **5**. Hydrogen atoms are omitted.

complexes **1**, **4**, and **5**, together with those computed for the archetypical complex $[Ir(ppy)_2(bpy)]^+$ (**A1**) for comparison purposes. Complexes **2** and **3** present identical molecular orbital topologies to those depicted in Figure 3 for **1**. As found for **A1**, the HOMO of **1**−**4** is mainly localized on the Ir center and the phenyl rings of the cyclometalating ligands, the main effect of the $ptrz^-$ ligands being the stabilization of the HOMO by ∼0.3 eV. This stabilization supports the higher oxidation potentials measured for **1**−**4** (around +1.15 V, Table 2) compared with **A1** (+0.84 V).[64] For complex **5**, the HOMO, which is also localized on the Ir-phenyl environment, is further stabilized (∼0.4 eV) by the electron-withdrawing effect of the *tert*-butyl isocyanide ligands. This additional stabilization explains the anodic shift (∼0.4 V) measured for the oxidation potential in passing from **1**−**4** to **5** (Table 2).

The cyclometalating $ptrz^-$ ligands have no special effect on the LUMO of complexes **1**−**4** because this orbital is located on the ancillary ligand (see Figure 3). The LUMO appears at very similar energies for **1** (−2.43 eV), **3** (−2.40 eV), and **A1** (−2.42 eV), justifying the almost identical values recorded for the first reduction potential of these complexes (−1.79, −1.77, and −1.77 V,[63] respectively). For **2**, the LUMO (−2.25 eV) is slightly destabilized by the electron-donating effect of the *tert*-butyl substituents in accord with the more cathodic reduction potential measured for this complex (−1.87 V). Substitution of a pyridine ring by a triazole ring in complex **4** causes a LUMO destabilization of 0.40 eV with respect to **1** (Figure 3), in accord with the cathodic shift of 0.44 V measured experimentally. The lack of low-energy π^* virtual orbitals in the isocyanide ligands determines that the LUMO of complex **5** relies on the tetrazole rings of the cyclometalating ligands and appears at high energies (−1.62 eV) compared to **1** (−2.43 eV). This justifies the cathodic shift of 0.72 V observed for the first reduction potential in passing from **1** to **5** (Table 2).

Theoretical calculations therefore predict that the HOMO−LUMO energy gap increases along the series **A1** (3.22 eV) < **1** (3.50 eV) ≈ **3** (3.53 eV) < **2** (3.65 eV) < **4** (3.90 eV) < **5** (4.75 eV). This series is in perfect agreement with the electrochemical gaps inferred from CV measurements (2.61, 2.94, 2.95, 3.00, 3.48, and 4.07 V, respectively). A noticeable blue shift is therefore expected in both absorption and emission properties in passing from **1**−**3** to **4** and especially to **5**.

Photophysical Properties in Solution. *Absorption Spectra.* The RT absorption spectra of complexes **1**−**5** in acetonitrile are reported in Figure 4; spectra in dichloromethane are depicted in Figure S2 in the Supporting Information. All complexes display high stability in both solvents for several weeks, under standard laboratory conditions.

The 200−275 nm spectral window is dominated by intense absorption bands ($\varepsilon \approx (2-7) \times 10^4$ M^{-1} cm^{-1}) that are

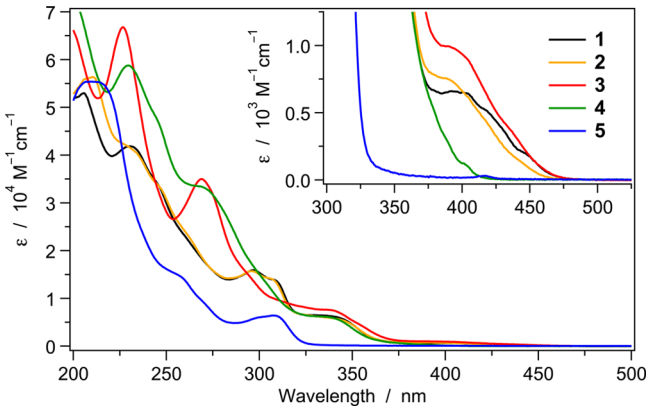

Figure 4. Absorption spectra of complexes **1**−**5** in acetonitrile at 298 K: **1** (black), **2** (orange), **3** (red), **4** (green), and **5** (blue). (inset) The direct transition $S_0 \rightarrow T_1$ is magnified.

dx.doi.org/10.1021/ic500999k | Inorg. Chem. 2014, 53, 7709−7721

assigned to spin-allowed ligand-centered (LC) $\pi-\pi^*$ transitions involving both the cyclometalating and the ancillary ligands. On the other hand, the weaker and broader bands at longer wavelengths (275−375 nm; $\varepsilon \approx (1-15) \times 10^3$ M^{-1} cm^{-1}) are attributed to charge transfer transitions with mixed metal-to-ligand and ligand-to-ligand charge transfer (MLCT/LLCT) character.[1] In the case of **5**, the absorption band at 325−350 nm is absent because isocyanide ancillary ligands do not have low-energy π^* acceptor orbitals allowing MLCT transitions from the iridium metal center; this is a common feature in cationic Ir(III) complexes with isocyanides.[22,23,26]

The weak and long tail observed in the spectra above 375 nm (inset, Figure 4) is due to direct spin-forbidden absorption from the singlet ground state (S_0) to the first triplet excited state (T_1) of the complexes, enabled by the high spin−orbit coupling constant of the iridium metal core (ζ_{Ir} = 3909 cm^{-1}). This band is stronger for **1**−**3** ($\varepsilon \approx (5-10) \times 10^2$ M^{-1} cm^{-1}) where T_1 is expected to have a marked MLCT character,[1] but is much less pronounced for **4**. On the other hand, it is completely absent in **5**, in agreement with the fact that isocyanide-based Ir(III) complexes lack MLCT transitions and, accordingly, display only strong ligand-centered (LC) luminescence.[22,23,26]

It is noteworthy that the phenyl-tetrazole cyclometalating ligands are capable of blue shifting not only the MLCT absorption transitions, but also the direct $S_0 \rightarrow T_1$ band. This can be observed in Figure 5, where the absorption spectra of

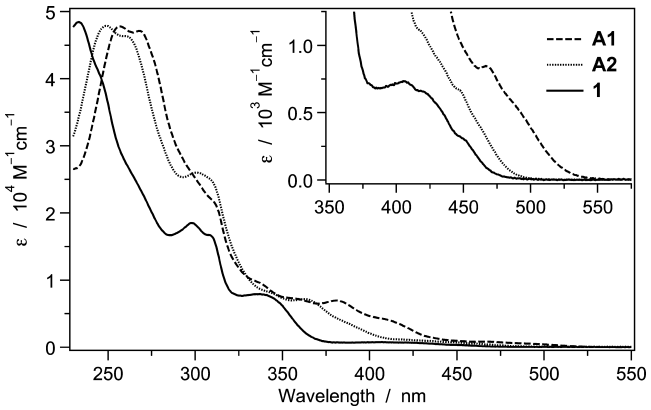

Figure 5. Absorption spectra in dichloromethane at 298 K of some archetypal Ir(III) complexes having the same ancillary ligand (2,2′-bypiridine) but different cyclometalating ligands: 2-methyl-5-phenyl-2*H*-tetrazole (**1**, full), 2-phenylpyridine (**A1**, dashed), and 2-(2,4-difluorophenyl)pyridine (**A2**, dotted). (inset) The $S_0 \rightarrow T_1$ transition is magnified to allow easy comparison.

two archetypal Ir-iTMCs widely used as emitters in LECs, namely, $[Ir(ppy)_2(bpy)]^+$ (**A1**) and $[Ir(dfppy)_2(bpy)]^+$ (**A2**), are compared to **1**; all complexes have the same ancillary ligand, but different cyclometalating units. The effect on the $S_0 \rightarrow T_1$ transition is particularly remarkable with respect to **A2**, because no electron-withdrawing fluorine substituents are present on the tetrazolate complex **1**.

Emission Properties. The emission spectra of **1**, **2**, **3**, and **5** at 298 K in acetonitrile are reported in Figure 6; spectra in dichloromethane are depicted in Figure S3 in the Supporting Information. The luminescence properties and photophysical parameters of **1**−**5** are summarized in Table 3; emission maxima can be compared to those of some selected archetypal complexes (**A**−**C**) gathered in Chart 2.

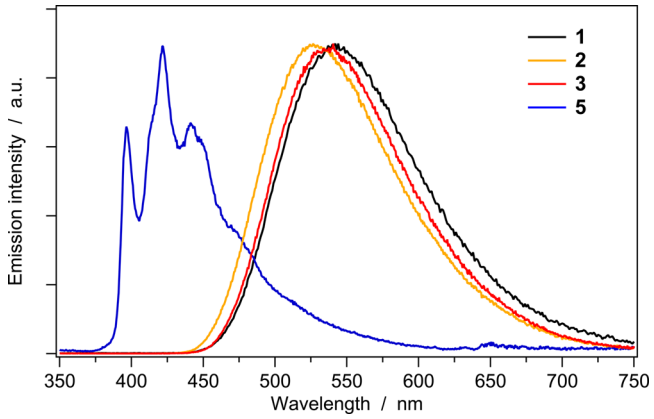

Figure 6. Normalized emission spectra of **1**, **2**, **3**, and **5** in acetonitrile solution at 298 K. **1**−**3** exhibit a broad and unstructured emission band underpinning MLCT character, while **5** shows an LC-type emission profile, typical of isocyanide-based iridium(III) complexes.

All the complexes of the tetrazole-based series display blue-green emission with maxima between 440 and 540 nm, that is, a range similar to polyfluorinated **A2**, **B2**, and **C2** (see Chart 2). Indeed, the strong-field cyclometalating $ptrz^-$ ligand is able to blue shift the T_1 emission even more strongly than the pristine ppz^- ligand is able to.

In line with the absorption spectra, **1**−**3** show similar emission properties with broad and structureless bands typical of a triplet T_1 state with strong MLCT character, while **5** exhibits a much bluer and more vibronically structured emission, clearly indicating an emitting triplet state of predominant LC character. Peculiarly, **4** is a very weak emitter, and the reasons for this behavior will be rationalized in the next section, with the support of quantum-chemical calculations.

The different nature of the emitting states is also crucially influencing the photoluminescence quantum yield (PLQY) of this family of complexes. Complexes **1**−**3** show very high PLQYs (up to 70%), whereas **5** is almost nonemissive (Φ_{em} = 0.5%). To the best of our knowledge, the PLQYs of **1**−**3** in RT solutions are the highest ever reported for fluorine-free cationic iridium(III) complexes having a bipyridine-type ancillary ligand. In fact, these PLQY values are only comparable to some polyfluorinated complexes[65] (e.g., **A2** and **C2** that exhibit PLQYs of 55%[41] and 73%,[34] respectively). Complexes **1**−**3** exhibit radiative constants similar to many others Ir-iTMCs ($k_r \approx 4 \times 10^5$ s^{-1}), so the high PLQY values are primarily attributable to the lack of effective nonradiative pathways. This picture drastically changes if the T_1 state does not have a pronounced MLCT character, as in the case of **5** (*vide infra*). For this complex, in which the lowest electronic state has an LC character, the radiative constant drastically drops by a factor of 100 ($k_r \approx 6 \times 10^3$ s^{-1}) and makes **5** barely emissive. The photophysical properties of **5** are very similar to those of $[Ir(ppz)_2(CN^tBu)_2]^+$ that have been reported recently.[26] Therefore, it can be concluded that 5-phenyltetrazole (ptrz), 1-phenylpyrazole (ppz), and phenyl-[1,2,3]triazole (phtl) cyclometalating ligands act in a very similar way in cationic iridium(III) complexes bearing high-field ancillary ligands, that is, they exhibit faint luminescence.[19,26,33] A totally different behavior is observed for $[Ir(ppy)_2(CN^tBu)_2]^+$ and analogous 2-phenylpyridine complexes, where, in spite of rather small k_r values ($(2-18) \times 10^3$ s^{-1}), very high PLQYs (~30−70%) were found.[22,23]

dx.doi.org/10.1021/ic500999k | *Inorg. Chem.* 2014, 53, 7709−7721

Table 3. Luminescence Properties and Photophysical Parameters of 1−5 in Solution at 298 and 77 K

	CH_3CN oxygen-free solution, 298 K					CH_2Cl_2 oxygen-free solution, 298 K					77 K rigid matrix, CH_3CN	
	λ_{em}[a] (nm)	Φ_{em}[a] (%)	τ[b] (ns)	k_r[c] (10^5 s^{-1})	k_{nr}[d] (10^5 s^{-1})	λ_{em}[e] (nm)	Φ_{em}[e] (%)	τ[b] (ns)	k_r[c] (10^5 s^{-1})	k_{nr}[d] (10^5 s^{-1})	λ_{em}[a] (nm)	τ[b] (μs)
1	545	54.8	1220	4.49	3.70	532	65.2	1267	5.15	2.75	450, 482, 505	3.7
2	530	67.6	1181	5.72	2.74	514	60.9	1077	5.65	3.63	442, 466, 500	3.6
3	540	70.3	1665	4.22	1.78	520	68.9	1547	4.45	2.01	462, 495, 530, 570	11.2
4	524	<0.1	*f*	*f*	*f*	524	~0.1	*f*	*f*	*f*	410, 436, 462	7.5
5	442	0.5	873	0.06	11.4	442	0.5	787	0.06	12.6	396, 422, 446	106

[a]λ_{exc} = 360 nm. [b]λ_{exc} = 407 nm. [c]Radiative constant: $k_r = \Phi_{em}/\tau$. [d]Nonradiative constant: $k_{nr} = 1/\tau - k_r$. [e]λ_{exc} = 375 nm. [f]Data not reported due to very low emission.

The most puzzling case is **4**, which bears a pyridine-triazole ancillary ligand. This complex exhibits a broad emission band similar to **1**−**3**, indicative of a T_1 level with a largely predominant MLCT character. However, the emission quantum yields in solution are extremely low (Φ_{em} < 0.1%, Table 3), that is, even smaller than **5**.

Theoretical Calculations: Triplet Excited States. In an attempt to rationalize the absorption and emission properties, the lowest triplet excited states of complexes **1**−**5** were first calculated at the optimized geometry of the ground state (S_0) using the time-dependent DFT (TD-DFT) approach. Table S3 in the Supporting Information lists the vertical excitation energies and the electronic descriptions computed for the three first triplet excited states. The lowest-energy triplet state (T_1) of complexes **1**, **2**, and **4** mainly results from the HOMO → LUMO excitation that implies an electron transfer from the Ir-ptrz environment, where the HOMO is localized, to the bpy ligand, where the LUMO resides (see Figure 3). The T_1 state therefore shows a mixed ^{3}MLCT/^{3}LLCT character. For complex **3**, the T_1 state is more multiconfigurational, but it also shows a ^{3}MLCT/^{3}LLCT character, and the HOMO → LUMO excitation gives rise to the T_2 state that is very close in energy to T_1. TD-DFT calculations predict the T_1 state at 2.79 eV (444 nm) for **1** and **3** and at 2.95 eV (421 nm) for **2**, in good agreement with the very weak bands observed in the 400−450 nm range of the absorption spectra (Figure 4, inset). For complex **4**, the T_1 state is calculated at higher energies (3.19 eV, 389 nm) due to the destabilization of the LUMO caused by the substitution of a pyridine ring by a triazole ring. This shift to lower wavelengths implies that the associated weak absorption band is hidden under the tail of the singlet absorption centered around 350 nm and is not observed in the experimental spectrum (Figure 4). Finally, for **5**, there is no low-energy MLCT triplet and, as expected, the T_1 state has a ^{3}LC character involving the cyclometalating ligands.

Calculations also rationalize the blue shift observed for the lowest-energy absorption band of **1** when compared with the archetype complexes $[Ir(ppy)_2(bpy)]^+$ (**A1**) and $[Ir(dfppy)_2(bpy)]^+$ (**A2**), which bear the same ancillary ligand (Figure 5). The $ptrz^-$ ligand brings about a shift of the $S_0 \rightarrow T_1$ transition to higher energies for **1** (2.79 eV, 444 nm) compared to **A1** (2.50 eV, 491 nm), which is even larger than that caused by the difluorinated $dfppy^-$ ligand in **A2** (2.74 eV, 451 nm).

Concerning the emission properties, TD-DFT calculations support the efficient and unstructured emission observed for complexes **1**−**3** based on the MLCT/LLCT nature of the T_1 state and the blue-shifted structured emission recorded for complex **5** due to the LC nature of T_1. However, they do not provide an explanation for the poor emission exhibited by complex **4**, for which T_1 is predicted to have the same electronic nature as **1**−**3**. To investigate this discrepancy, the lowest triplet excited states of complexes **1**−**5** were further examined by optimizing their geometry using the spin-unrestricted UB3LYP approach.

The relative energy position and unpaired-electron spin density distributions calculated for the lowest-energy triplets of complexes **1** and **4** are depicted in Figure 7. After full-geometry relaxation, the T_1 state is computed to lie 2.63 eV above S_0 for **1** and 3.03 eV above S_0 for **4** (adiabatic energy differences, $\Delta E(T_1 - S_0)$ in Figure 7). The spin-density distribution calculated for both **1** (Ir: 0.49e, C^N ligands: 0.48e, N^N ligand: 1.03e) and **4** (Ir: 0.47e, C^N ligands: 0.50e, N^N ligand: 1.03e) perfectly matches the topology of the HOMO → LUMO excitation (Figure 3) and confirms the electron transfer from the Ir-ptrz environment to the ancillary ligand, that is, the ^{3}MLCT/^{3}LLCT character of T_1. The T_2 state corresponds in both cases to a ^{3}LC state. For **1**, the T_2 state is localized over the ancillary $\hat{N}N$ ligand and is calculated 0.21 eV above T_1. By contrast, in **4**, T_2 is centered on one of the C^N ligands and is mostly degenerate with T_1 ($\Delta E(T_2 - T_1)$ = 0.01 eV).

The most important difference between **1** and **4** is that for the latter a metal-centered (^{3}MC) state, in which the Ir center accumulates a large part of the unpaired electrons (Ir: 1.23e, C^N ligands: 0.65e, N^N ligand: 0.13e), appears 0.21 eV below T_1 (Figure 7b). This ^{3}MC state implies the decoordination of the pyridine ring that twists around the inter-ring bond and moves away from the iridium center (Ir−N_{pyr} distance = 3.4 Å, Table S2 in the Supporting Information). A similar behavior was found for complexes incorporating pyridine-carbene ancillary ligands,[66,67] with formation of a pentacoordinated iridium center. For complex **1**, all of the attempts made to localize the ^{3}MC state invariably led to a related description implying the nitrogen atoms of the bpy ligand moving away from the Ir center (2.5 Å) but still coordinated. The resulting ^{3}MC state (Ir: 1.17e, C^N ligands: 0.64e, N^N ligand: 0.18e) is calculated 0.33 eV above T_1 (Figure 7a). The larger structural distortion found in the ^{3}MC state of **4** is due to the asymmetric nature of the taz N^N ligand that favors the preferred decoordination of the pyridine ring. The Ir−N distances calculated for the S_0 state of **4** (Ir−N_{pyr} = 2.235 Å, Ir−$N_{triazol}$ = 2.175 Å, Supporting Information, Table S2) actually indicate that the pyridine ring is less strongly attached to the iridium center than the triazol ring. In contrast, in complex **1** the two nitrogen atoms of the N^N ligand (bpy) are equally coordinated to the iridium center, and they prefer to move away from Ir in a synchronous way in the ^{3}MC state. Therefore, emission in **1** originates from the lowest-energy HOMO → LUMO T_1 state of the ^{3}MLCT/^{3}LLCT character. The emission

dx.doi.org/10.1021/ic500999k | Inorg. Chem. 2014, 53, 7709−7721

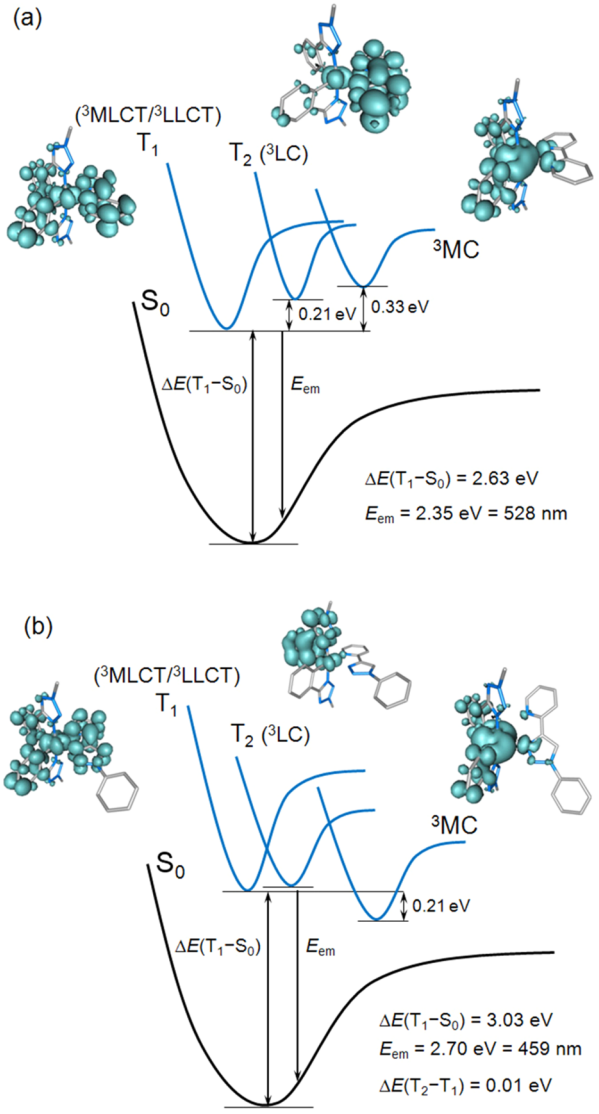

Figure 7. Schematic energy diagram showing the adiabatic energy differences (ΔE) between S_0 and the lowest triplet states and the emission energy (E_{em}) from T_1 calculated for (a) **1** and (b) **4**. The unpaired-electron spin-density contours (0.003 au) calculated for the fully relaxed triplet states are depicted together with the electronic nature of the states.

energy of T_1 (528 nm), calculated as the vertical energy difference between T_1 and S_0 at the optimized minimum-energy geometry of T_1 (E_{em} in Figure 7a), is in good agreement with experiment (545 nm in CH_3CN and 532 nm in CH_2Cl_2). For **2** and **3** the triplet state distribution is similar to that obtained for **1**, and emission also takes place from the ^{3}MLCT/^{3}LLCT T_1 state.

Notably, the energy distribution of the triplet states calculated for **4** is completely different. The T_1 (^{3}MLCT/^{3}LLCT) and T_2 (^{3}LC centered on the C^N ligands) states are almost degenerate, and a lower-energy ^{3}MC state is present, which opens a deactivation pathway to S_0. At its minimum-energy geometry, the ^{3}MC state is indeed calculated to be only 0.33 eV above S_0, which facilitates the nonemissive deactivation of **4** once the ^{3}MC state is populated. Theoretical calculations therefore suggest that, at RT, the low-energy ^{3}MC state largely quenches the emission of complex **4**, justifying the low PLQYs experimentally measured. The observed weak and unstructured emission band of **4** likely stems from the ^{3}MLCT/^{3}LLCT state T_1. To further support the different energy ordering found for the excited states in complexes **1** and **4**, the geometry of the triplet states was reoptimized at the more accurate TD-DFT level. TD-DFT calculations predict that the ^{3}MC state in complex **4** lies lower in energy than T_1 by 0.37 eV, while for complex **1** it resides 0.38 eV above the emitting T_1 state, thus confirming the ordering shown in Figure 7.

Low-Temperature and Thin-Film Photophysical Properties. To get a wider understanding of the photophysical properties of complexes **1**–**5**, we performed luminescence experiments at 77 K. Spectral data and lifetimes are summarized in Table 3, and emission bands are collected in Figure 8. In

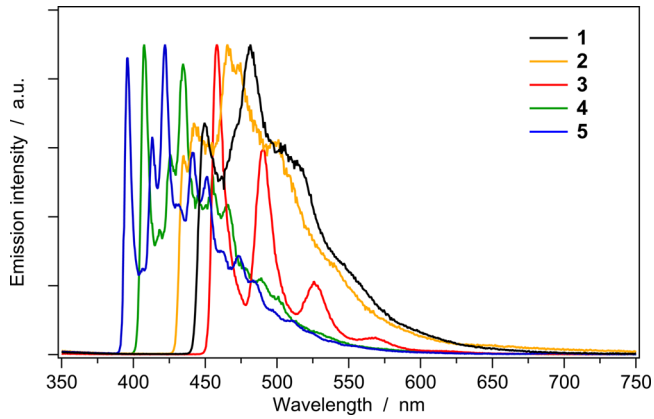

Figure 8. Normalized 77 K emission spectra of complexes **1**–**5** recorded in frozen acetonitrile matrix.

rigid matrix at 77 K, all complexes exhibit bright emissions of comparable intensity when excited at the same experimental conditions. Therefore, also **4** and **5**, which are very poor emitters at 298 K, show intense luminescence at low temperature.

In line with previous findings on Ir(III) complexes,[21,28] **1** and **2** (T_1 state with a strong MLCT character) exhibit more structured emission profiles and undergo a considerable blue shift (around 50 nm, passing from 298 to 77 K) due to rigidochromic effects. On the other hand, **5** displays an emission spectrum that is not temperature-dependent, further corroborating the LC nature of its T_1 state, with emission mainly centered on the cyclometalating ligand (Figure 9a).

A dramatic change in the spectral shape (i.e., electronic nature) and emission intensity from 298 to 77 K is observed for ligand **4**. At 77 K, population of the ^{3}MC state is prevented because the frozen medium inhibits the rotation of the pyridine ring required for the relaxation of this state (see above).

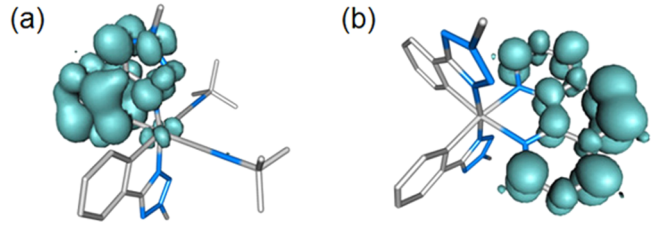

Figure 9. Unpaired-electron spin-density contours (0.003 au) calculated for (a) the T_1 state of **5** and (b) the T_2 state of **3**.

dx.doi.org/10.1021/ic500999k | Inorg. Chem. 2014, 53, 7709–7721

Therefore, at low temperature, emission from the almost degenerate T_1 and T_2 states (Figure 7b) is not quenched by the ^{3}MC state. In addition, T_1 and T_2 split at low temperature, that is, the polar MLCT/LLCT state moves to higher energies (similarly to **1** and **2**) due the blocking of the solvent reorganization at 77 K, whereas the apolar LC level (centered on the cyclometalating ligands as in **5**) remains substantially unaffected. As a result, the 77 K emission band of **4** shows the same complex vibronic progressions of **5**, though it is located at lower energy due to the smaller d−d orbital splitting of pyridine-triazole with respect to isocyanide ligands (Supporting Information, Figure S4). The different nature of the emitting level of **4** versus **1** and **2** at 77 K (LC vs MLCT) is likely at the origin of its longer excited-state lifetime (Table 3).

The longer lifetime of **3** at 77 K with respect to **1**, **2**, and **4** can be rationalized through the triplet state ordering predicted for this phenanthroline-based complex. As discussed above, **3** shows the same triplet distribution depicted in Figure 7a for **1**. That is, T_1 corresponds to the HOMO → LUMO ^{3}MLCT/^{3}LLCT state, and T_2 is a ^{3}LC state centered on the phenanthroline ancillary ligand (Figure 9b); they are separated by only 0.10 eV. In analogy with **4** (see above), at 77 K we can assume that the LC state becomes the lowest-lying because of the energy increase of the MLCT/LLCT state, due to rigidochromic effects. These theoretical findings are corroborated by the 77 K emission profile of **3**, which is practically superimposable onto that of pristine phen under the same conditions.[68] Indeed, the spin density distribution depicted in Figure 9b fully corresponds to that calculated for the first triplet state of phen.

The new series of Ir(III) tetrazolate complexes was ultimately designed and prepared to open a new route for green/blue highly luminescent Ir emitters for light-emitting electrochemical cells (LECs) without fluorine-containing ligands. Therefore, we also investigated the emission properties of **1**−**5** in the solid state, that is, dispersed in a poly(methyl methacrylate) (PMMA) matrix at a concentration of 1% by weight and as neat films. Table 4 and Figure 10 collect the

Table 4. Luminescence Properties of 1−3 at 298 K in the Solid State

	1% PMMA matrix			neat film		
	λ_{em}[a] (nm)	Φ_{em}[a] (%)	τ[b] (μs)	λ_{em}[a] (nm)	Φ_{em}[a] (%)	τ[b] (ns)
1	490	69	1.1	520	45	537
2	485	51	1.0	527	70	774
3	497	57	2.6	535	27	650

[a] λ_{exc} = 310 nm. [b] λ_{exc} = 407 nm.

experimental data obtained for complexes **1**−**3** only, which exhibited PLQYs in the range of ∼30−70%, unlike **4** and **5**, which have PLQYs below 5%. The similar emission behavior of **4** and **5** under these conditions is not surprising because in rigid PMMA matrix the ^{3}MC state of **4** cannot fully relax and is no longer the lowest one. Therefore, in both cases, the lowest excited state is of ^{3}LC nature, which is typically poorly emissive in the presence of a 5-membered heteroatomic ring on the cyclometalated ligand.[26] As far as the photophysical data in Table 4 are concerned, notice that **1** and **2** exhibit similar values of the radiative constant ($k_r = \Phi/\tau$) in PMMA ($5 \div 6 \times 10^5$ s^{-1}), which are also comparable to those in CH_3CN and CH_2Cl_2 (Table 3). By contrast, the rate constant of **3** is lower

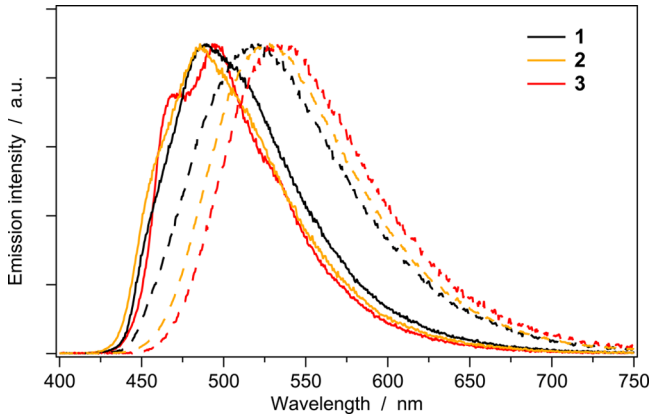

Figure 10. Normalized emission spectra of complexes **1**−**3** in the solid state at 298 K. Full lines: in 1% PMMA matrix; dashed lines: in neat film.

with respect to **1** and **2** in both media. The k_r value of **3** is particularly low in PMMA (2.2×10^5 s^{-1}), as a consequence of a longer lifetime, which might reflect a slightly different character of the triplet level, with some LC character. This is in line with 77 K phosphorescence data that show an unusually long phosphorescence lifetime of 11.2 μs in CH_3CN at 77 K for **3** (Table 3). On the other hand, a comparison of highly dilute samples with neat films is not appropriate due to the intermolecular interactions occurring in the latter. However, notice that **3** exhibits the smallest radiative rate constant also in neat films, that is, 4.2×10^5 s^{-1}, compared to $\sim 9 \times 10^5$ s^{-1} for **1** and **2**.

LEC Devices. As mentioned in the Introduction, it is very challenging to obtain solid-state electrophosphorescent devices at high energy, that is, emitting in the blue region. This is especially the case for LECs, where the transition-metal complex is responsible not only for the emission of light but also for the transport of electrons and holes throughout the film. We have selected complex **2**, due to its superior PLQY in neat film, to prepare LECs following the procedure described in detail in the Supporting Information.

The electroluminescence spectra of such devices are very similar to those obtained by photoexcitation in neat films with an emission maximum at 552 nm. The devices were driven by a pulsed current using a block wave at a frequency of 1 kHz with a duty cycle of 50% and an average current density of 100 A m^{-2}. These operative conditions were previously shown to enhance the performances of LECs.[69] LECs built up with **2** reach a maximum luminance of 310 cd m^{-2} that drops within 2 h to 20 cd m^{-2} (Figure 11). The luminance observed is among the best observed for blue-emitting LECs. The efficiency is low, and the stability is similar to many blue-emitting LECs.[1]

Therefore, the devices operate with reasonable efficiency, but the performance is rapidly decreasing, probably due to undesired quenching of the excited state caused by a recombination at one of the extremes of the light-emitting layer. This can be inferred from the average voltage versus time curve, which decreases quickly over the first minutes and continues decreasing at longer time scales (Figure 11). It was demonstrated that the initial decrease is caused by the reduction of the injection barriers as ions accumulate at the interface with the electrodes.[70]

Once electrons and holes are injected in the light-emitting material in the presence of uncompensated ions, some of the

dx.doi.org/10.1021/ic500999k | Inorg. Chem. 2014, 53, 7709−7721

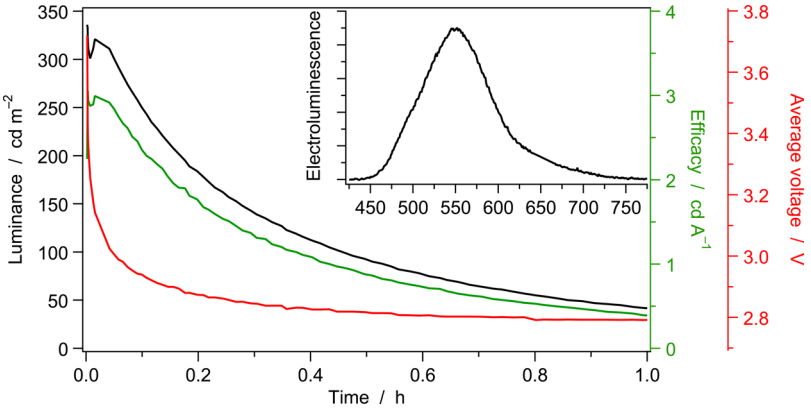

Figure 11. Luminance, average driving voltage, and efficacy for a LEC using **2** as phosphorescent material, which is driven by a pulsed current of 100 A m^{-2} (1000 Hz, 50% duty cycle, block wave). (inset) The electroluminescence spectrum of the device obtained under these driving conditions.

electronic charges get compensated by the ionic charges. The compensation of excess electrons on the iridium complexes by the uncompensated positive ions leads to the formation of electrochemically doped layers. These doped layers are beneficial for charge injection and transport, as the conductivity of these zones is significantly higher than the intrinsic (nondoped) layers. Hence, the remaining potential drops over the nondoped region that is thinner than the original light-emitting layer. This process is reflected in the continued slow decrease of the average voltage versus time, as less voltage is needed to maintain a current density over a thinning intrinsic layer. An additional, less desirable effect of the doped layers is their capability to quench excited states. Hence, with rapidly expanding doped zones, the number of quenched excited states is increased, leading to the reduction of the luminance and, consequently, of the efficacy. Hence, to summarize the performance in electroluminescent devices, complex **2** is able to simultaneously transport electrons and holes and leads to efficient luminescence with an emission spectrum similar to that observed under photoexcitation. The observed low stability is most likely related to unbalanced charge transport within the device.[1]

CONCLUSION

The first cationic Ir(III) complexes with tetrazole units on the C^N cyclometallating ligand (**1**−**5**, $[Ir(ptrz)_2(L^L)]^+$, Hptrz = 2-methyl-5-phenyl-2*H*-tetrazole) have been synthesized and fully characterized. The presence of four nitrogen atoms on the five-membered ring makes tetrazole a stronger electron donor compared to its analogues pyrazole and triazole. Accordingly, stabilization of the HOMO of the $[Ir(ptrz)_2(L^L)]^+$ complexes is attained, enhancing the ligand field and pushing the emission to the blue. This strategy had proved effective in the past, with blue shift of the luminescence by passing from complexes containing 2-phenylpyridine to 1-phenylpyrazole.[28] Indeed, $[Ir(C^N)_2(L^L)]^{0/+}$ complexes with triazole units on the C^N ligands were also made but, surprisingly, they proved unsuccessful in promoting further emission to blue shift relative to pyrazole counterparts.[34]

In this context, the ultimate step to increase the nitrogen atoms on the C^N ligand, that is, the use of 5-phenyltetrazoles, had remained unexplored, because the classic protocol to prepare cyclometalated Ir(III) complexes, based on the preliminary formation of the μ-dichloro-bridged dimer $[(C^N)_2Ir(\mu\text{-}Cl)]_2$, is ineffective with tetrazoles. To address this problem, we have designed a novel two-step synthetic strategy based on a silver-assisted cyclometalation reaction with $IrCl_3$ that afforded tetrazolate complexes **1**−**5** with medium-to-high yields (40−75%).

Our primary goal to blue shift the emission of cationic Ir(III) complexes through the modification of the C^N ligand, while keeping an electronic transition with predominant charge transfer character, was fully accomplished with compounds **1**−**3**, which exhibit the highest-energy MLCT/LLCT emission bands ever reported for fluorine-free cyclometalating ligands. They display green-bluish photoluminescence, with quantum yields in the range of 55−70% in acetonitrile at RT. Similar PLQY values are found in solid matrices, making **1**−**3** suitable for LEC device testing. The strongest emitter in neat films (**2**) was tested and afforded good quality films with remarkable maximum luminance (310 cd m^{-2}) but limited stability.

This paper discloses a novel synthetic strategy to an unprecedented class of cationic iridium cyclometalated complexes. Chemical modifications of the tetrazole ligands will now offer the possibility to further push the emission band toward the blue, presently one of the most important goals in this area of investigation. Moreover, based on the deep understanding of the electronic and photophysical properties of **1**−**5** acquired through experimental and theoretical methods, we now aim to design cationic Ir-tetrazolate complexes with tailored features for easy device preparation and enhanced electroluminescence performance.

ASSOCIATED CONTENT

Supporting Information

Full experimental details of the electrochemical, theoretical, photophysical and device part; ^{1}H NMR, ^{13}C NMR, and mass spectra (ESI) of all complexes; crystal data for **P**, **2** and **3**; cyclic voltammograms of **1** recorded at different scan rates; DFT and TD-DFT data regarding bond distances and angles (S_0, T_1, and ^{3}MC) and triplet vertical excitations; absorption and emission spectra in dichloromethane solution. This material is available free of charge via the Internet at http://pubs.acs.org.

AUTHOR INFORMATION

Corresponding Authors

*E-mail: enrique.orti@uv.es. (E.O.)
*E-mail: letizia.sambri@unibo.it. (L.S.)
*E-mail: nicola.armaroli@isof.cnr.it. (N.A.)

Notes

The authors declare no competing financial interest.

■ ACKNOWLEDGMENTS

This work was supported by the Italian Ministry of Research (MIUR) (PRIN 2010 INFOCHEM, Contract No. CX2TLM; FIRB Futuro in Ricerca SUPRACARBON, Contract No. RBFR10DAK6), UNIBO-RFO, the Consiglio Nazionale delle Ricerche (CNR) (MACOL PM. P04. 010, and Progetto Bandiera N−CHEM), the Spanish Ministry of Economy and Competitiveness (MINECO) (MAT2011-24594 and CTQ2012-31914), the Generalitat Valenciana (PROMETEO/2012/053), and European FEDER funds (CTQ2012-31914). A.P. acknowledges the MINECO for an FPI grant.

■ REFERENCES

(1) Costa, R. D.; Ortí, E.; Bolink, H. J.; Monti, F.; Accorsi, G.; Armaroli, N. *Angew. Chem., Int. Ed.* **2012**, *51*, 8178.
(2) Chou, P. T.; Chi, Y. *Chem.—Eur. J.* **2007**, *13*, 380.
(3) Evans, R. C.; Douglas, P.; Winscom, C. J. *Coord. Chem. Rev.* **2006**, *250*, 2093.
(4) Gather, M. C.; Köhnen, A.; Meerholz, K. *Adv. Mater.* **2011**, *23*, 233.
(5) Hu, T.; He, L.; Duan, L.; Qiu, Y. *J. Mater. Chem.* **2012**, 4206.
(6) Lowry, M. S.; Bernhard, S. *Chem.—Eur. J.* **2006**, *12*, 7970.
(7) Wang, J.; Zhang, F.; Zhang, J.; Tang, W.; Tang, A.; Peng, H.; Xu, Z.; Teng, F.; Wang, Y. *J. Photochem. Photobiol. C* **2013**, *17*, 69.
(8) Flamigni, L.; Barbieri, A.; Sabatini, C.; Ventura, B.; Barigelletti, F. *Top. Curr. Chem.* **2007**, *281*, 143.
(9) Slinker, J.; Bernards, D.; Houston, P. L.; Abruña, H. D.; Bernhard, S.; Malliaras, G. G. *Chem. Commun.* **2003**, 2392.
(10) Slinker, J. D.; Koh, C. Y.; Malliaras, G. G.; Lowry, M. S.; Bernhard, S. *Appl. Phys. Lett.* **2005**, *86*.
(11) Slinker, J. D.; Gorodetsky, A. A.; Lowry, M. S.; Wang, J. J.; Parker, S.; Rohl, R.; Bernhard, S.; Malliaras, G. G. *J. Am. Chem. Soc.* **2004**, *126*, 2763.
(12) Xiao, L.; Chen, Z.; Qu, B.; Luo, J.; Kong, S.; Gong, Q.; Kido, J. *Adv. Mater.* **2011**, *23*, 926.
(13) *Organic Light-Emitting Diodes (OLEDs). Materials, Devices and Applications;* Buckley, A., Ed.; Woodhead Publishing: Cambridge, U.K., 2013.
(14) Li, J.; Djurovich, P. I.; Alleyne, B. D.; Yousufuddin, M.; Ho, N. N.; Thomas, J. C.; Peters, J. C.; Bau, R.; Thompson, M. E. *Inorg. Chem.* **2005**, *44*, 1713.
(15) Rausch, A. F.; Thompson, M. E.; Yersin, H. *J. Phys. Chem. A* **2009**, *113*, 5927.
(16) Ladouceur, S.; Zysman-Colman, E. *Eur. J. Inorg. Chem.* **2013**, 2985.
(17) Stagni, S.; Colella, S.; Palazzi, A.; Valenti, G.; Zacchini, S.; Paolucci, F.; Marcaccio, M.; Albuquerque, R. Q.; De Cola, L. *Inorg. Chem.* **2008**, *47*, 10509.
(18) Yang, C.-H.; Li, S.-W.; Chi, Y.; Cheng, Y.-M.; Yeh, Y.-S.; Chou, P.-T.; Lee, G.-H.; Wang, C.-H.; Shu, C.-F. *Inorg. Chem.* **2005**, *44*, 7770.
(19) Sajoto, T.; Djurovich, P. I.; Tamayo, A. B.; Oxgaard, J.; Goddard, W. A.; Thompson, M. E. *J. Am. Chem. Soc.* **2009**, *131*, 9813.
(20) Kozhevnikov, V. N.; Dahms, K.; Bryce, M. R. *J. Org. Chem.* **2011**, *76*, 5143.
(21) Costa, R. D.; Monti, F.; Accorsi, G.; Barbieri, A.; Bolink, H. J.; Ortí, E.; Armaroli, N. *Inorg. Chem.* **2011**, *50*, 7229.
(22) Shavaleev, N. M.; Monti, F.; Costa, R. D.; Scopelliti, R.; Bolink, H. J.; Ortí, E.; Accorsi, G.; Armaroli, N.; Baranoff, E.; Grätzel, M.; Nazeeruddin, M. K. *Inorg. Chem.* **2012**, *51*, 2263.
(23) Shavaleev, N. M.; Monti, F.; Scopelliti, R.; Armaroli, N.; Grätzel, M.; Nazeeruddin, M. K. *Organometallics* **2012**, *31*, 6288.
(24) Fernandez-Hernandez, J. M.; Ladouceur, S.; Shen, Y.; Iordache, A.; Wang, X.; Donato, L.; Gallagher-Duval, S.; de Anda Villa, M.; Slinker, J. D.; De Cola, L.; Zysman-Colman, E. *J. Mater. Chem. C* **2013**, *1*, 7440.
(25) Yang, C.-H.; Mauro, M.; Polo, F.; Watanabe, S.; Muenster, I.; Fröhlich, R.; De Cola, L. *Chem. Mater.* **2012**, *24*, 3684.
(26) Shavaleev, N. M.; Monti, F.; Scopelliti, R.; Baschieri, A.; Sambri, L.; Armaroli, N.; Grätzel, M.; Nazeeruddin, M. K. *Organometallics* **2013**, *32*, 460.
(27) Grushin, V. V.; Herron, N.; LeCloux, D. D.; Marshall, W. J.; Petrov, V. A.; Wang, Y. *Chem. Commun.* **2001**, 1494.
(28) Tamayo, A. B.; Garon, S.; Sajoto, T.; Djurovich, P. I.; Tsyba, I. M.; Bau, R.; Thompson, M. E. *Inorg. Chem.* **2005**, *44*, 8723.
(29) Ho, M.-L.; Hwang, F.-M.; Chen, P.-N.; Hu, Y.-H.; Cheng, Y.-M.; Chen, K.-S.; Lee, G.-H.; Chi, Y.; Chou, P.-T. *Org. Biomol. Chem.* **2006**, *4*, 98.
(30) He, L.; Duan, L.; Qiao, J.; Dong, G.; Wang, L.; Qiu, Y. *Chem. Mater.* **2010**, *22*, 3535.
(31) Baranoff, E.; Fantacci, S.; De Angelis, F.; Zhang, X.; Scopelliti, R.; Grätzel, M.; Nazeeruddin, M. K. *Inorg. Chem.* **2011**, *50*, 451.
(32) Lai, W.-Y.; Levell, J. W.; Jackson, A. C.; Lo, S.-C.; Bernhardt, P. V.; Samuel, I. D. W.; Burn, P. L. *Macromolecules* **2010**, *43*, 6986.
(33) Beyer, B.; Ulbricht, C.; Escudero, D.; Friebe, C.; Winter, A.; Gonzalez, L.; Schubert, U. S. *Organometallics* **2009**, *28*, 5478.
(34) Ladouceur, S.; Fortin, D.; Zysman-Colman, E. *Inorg. Chem.* **2011**, *50*, 11514.
(35) Fernández-Hernández, J. M.; Yang, C.-H.; Beltrán, J. I.; Lemaur, V.; Polo, F.; Fröhlich, R.; Cornil, J.; De Cola, L. *J. Am. Chem. Soc.* **2011**, *133*, 10543.
(36) de Barros e Silva Botelho, M.; Fernandez-Hernandez, J. M.; de Queiroz, T. B.; Eckert, H.; De Cola, L.; de Camargo, A. S. S. *J. Mater. Chem.* **2011**, *21*, 8829.
(37) Fernández-Hernández, J. M.; Beltrán, J. I.; Lemaur, V.; Gálvez-López, M.-D.; Chien, C.-H.; Polo, F.; Orselli, E.; Fröhlich, R.; Cornil, J.; De Cola, L. *Inorg. Chem.* **2013**, *52*, 1812.
(38) Donato, L.; Abel, P.; Zysman-Colman, E. *Dalton Trans.* **2013**, *42*, 8402.
(39) Kiplinger, J. L.; Richmond, T. G.; Osterberg, C. E. *Chem. Rev.* **1994**, *94*, 373.
(40) Sivasubramaniam, V.; Brodkorb, F.; Hanning, S.; Loebl, H. P.; van Elsbergen, V.; Boerner, H.; Scherf, U.; Kreyenschmidt, M. *J. Fluorine Chem.* **2009**, *130*, 640.
(41) Constable, E. C.; Neuburger, M.; Rosel, P.; Schneider, G. E.; Zampese, J. A.; Housecroft, C. E.; Monti, F.; Armaroli, N.; Costa, R. D.; Ortí, E. *Inorg. Chem.* **2013**, *52*, 885.
(42) Thomas, E. W.; Cudahy, M. M. *J. Org. Chem.* **1993**, *58*, 1623.
(43) Lamansky, S.; Djurovich, P.; Murphy, D.; Abdel-Razzaq, F.; Kwong, R.; Tsyba, I.; Bortz, M.; Mui, B.; Bau, R.; Thompson, M. E. *Inorg. Chem.* **2001**, *40*, 1704.
(44) Tamayo, A. B.; Alleyne, B. D.; Djurovich, P. I.; Lamansky, S.; Tsyba, I.; Ho, N. N.; Bau, R.; Thompson, M. E. *J. Am. Chem. Soc.* **2003**, *125*, 7377.
(45) Nonoyama, M. *Bull. Chem. Soc. Jpn.* **1974**, *47*, 767.
(46) Lamansky, S.; Djurovich, P.; Murphy, D.; Abdel-Razzaq, F.; Lee, H. E.; Adachi, C.; Burrows, P. E.; Forrest, S. R.; Thompson, M. E. *J. Am. Chem. Soc.* **2001**, *123*, 4304.
(47) Henderson, W. *Adv. Organomet. Chem.* **2006**, *54*, 207.
(48) Butler, R. N. *Comprehensive Heterocyclic Chemistry II;* Storr, R. C., Ed.; Pergamon Press: Oxford, U.K., 1996; Vol. *4*, p 621.
(49) Stagni, S.; Palazzi, A.; Zacchini, S.; Ballarin, B.; Bruno, C.; Marcaccio, M.; Paolucci, F.; Monari, M.; Carano, M.; Bard, A. J. *Inorg. Chem.* **2006**, *45*, 695.
(50) Zhao, N.; Wu, Y.-H.; Shi, L.-X.; Lin, Q.-P.; Chen, Z.-N. *Dalton Trans.* **2010**, *39*, 8288.
(51) Lee, P.-K.; Liu, H.-W.; Yiu, S.-M.; Louie, M.-W.; Lo, K. K.-W. *Dalton Trans.* **2011**, *40*, 2180.
(52) Bandini, M.; Bianchi, M.; Valenti, G.; Piccinelli, F.; Paolucci, F.; Monari, M.; Umani-Ronchi, A.; Marcaccio, M. *Inorg. Chem.* **2010**, *49*, 1439.
(53) Ladouceur, S.; Fortin, D.; Zysman-Colman, E. *Inorg. Chem.* **2010**, *49*, 5625.

(54) Shavaleev, N. M.; Scopelliti, R.; Gratzel, M.; Nazeeruddin, M. K.; Pertegas, A.; Roldan-Carmona, C.; Tordera, D.; Bolink, H. J. *J. Mater. Chem. C* **2013**, *1*, 2241.
(55) Routledge, J. D.; Hallett, A. J.; Platts, J. A.; Horton, P. N.; Coles, S. J.; Pope, S. J. A. *Eur. J. Inorg. Chem.* **2012**, *2012*, 4065.
(56) Costa, R. D.; Ortí, E.; Bolink, H. J.; Graber, S.; Housecroft, C. E.; Neuburger, M.; Schaffner, S.; Constable, E. C. *Chem. Commun.* **2009**, 2029.
(57) Hanss, D.; Freys, J. C.; Bernardinelli, G.; Wenger, O. S. *Eur. J. Inorg. Chem.* **2009**, *2009*, 4850.
(58) Helms, M.; Lin, Z.; Gong, L.; Harms, K.; Meggers, E. *Eur. J. Inorg. Chem.* **2013**, *2013*, 4164.
(59) Su, H.-C.; Chen, H.-F.; Fang, F.-C.; Liu, C.-C.; Wu, C.-C.; Wong, K.-T.; Liu, Y.-H.; Peng, S.-M. *J. Am. Chem. Soc.* **2008**, *130*, 3413.
(60) Felici, M.; Contreras-Carballada, P.; Vida, Y.; Smits, J. M. M.; Nolte, R. J. M.; De Cola, L.; Williams, R. M.; Feiters, M. C. *Chem.—Eur. J.* **2009**, *15*, 13124.
(61) Juris, A.; Balzani, V.; Barigelletti, F.; Campagna, S.; Belser, P.; von Zelewsky, A. *Coord. Chem. Rev.* **1988**, *84*, 85.
(62) Armaroli, N. *Chem. Soc. Rev.* **2001**, *30*, 113.
(63) Tordera, D.; Bünzli, A. M.; Pertegás, A.; Junquera-Hernández, J. M.; Constable, E. C.; Zampese, J. A.; Housecroft, C. E.; Ortí, E.; Bolink, H. J. *Chem.—Eur. J.* **2013**, *19*, 8597.
(64) Costa, R. D.; Ortí, E.; Tordera, D.; Pertegás, A.; Bolink, H. J.; Graber, S.; Housecroft, C. E.; Sachno, L.; Neuburger, M.; Constable, E. C. *Adv. Energy Mater.* **2011**, *1*, 282.
(65) Bolink, H. J.; Coronado, E.; Costa, R. D.; Lardies, N.; Ortí, E. *Inorg. Chem.* **2008**, *47*, 9149.
(66) Kessler, F.; Costa, R. D.; Di Censo, D.; Scopelliti, R.; Ortí, E.; Bolink, H. J.; Meier, S.; Sarfert, W.; Gratzel, M.; Nazeeruddin, M. K.; Baranoff, E. *Dalton Trans.* **2012**, *41*, 180.
(67) Monti, F.; Kessler, F.; Delgado, M.; Frey, J.; Bazzanini, F.; Accorsi, G.; Armaroli, N.; Bolink, H. J.; Ortí, E.; Scopelliti, R.; Nazeeruddin, M. K.; Baranoff, E. *Inorg. Chem.* **2013**, *52*, 10292.
(68) Armaroli, N.; De Cola, L.; Balzani, V.; Sauvage, J. P.; Dietrich-Buchecker, C. O.; Kern, J. M. *J. Chem. Soc., Faraday Trans.* **1992**, *88*, 553.
(69) Tordera, D.; Meier, S.; Lenes, M.; Costa, R. D.; Ortí, E.; Sarfert, W.; Bolink, H. J. *Adv. Mater.* **2012**, *24*, 854.
(70) Lenes, M.; Garcia-Belmonte, G.; Tordera, D.; Pertegás, A.; Bisquert, J.; Bolink, H. J. *Adv. Funct. Mater.* **2011**, *21*, 1581.